

World In Your Hands: A Large-Scale and Open-source Ecosystem for Learning Human-centric Manipulation in the Wild

TARS Robotics, Yupeng Zheng*, Jichao Peng*, Weize Li, Yuhang Zheng, Xiang Li, Yujie Jin, Julong Wei, Guanhua Zhang, Ruiling Zheng, Ming Cao, Songen Gu, Zhenhong Zou, Kaige Li, Ke Wu, Mingmin Yang, Jiahao Liu, Pengfei Li, Hengjie Si, Feiyu Zhu, Wang Fu, Likun Wang, Ruiwen Yao, Jieru Zhao, Yilun Chen, Wenchao Ding†

Project Page: <https://wiyh.tars-ai.com>

Code: <https://github.com/tars-robotics/World-In-Your-Hands>

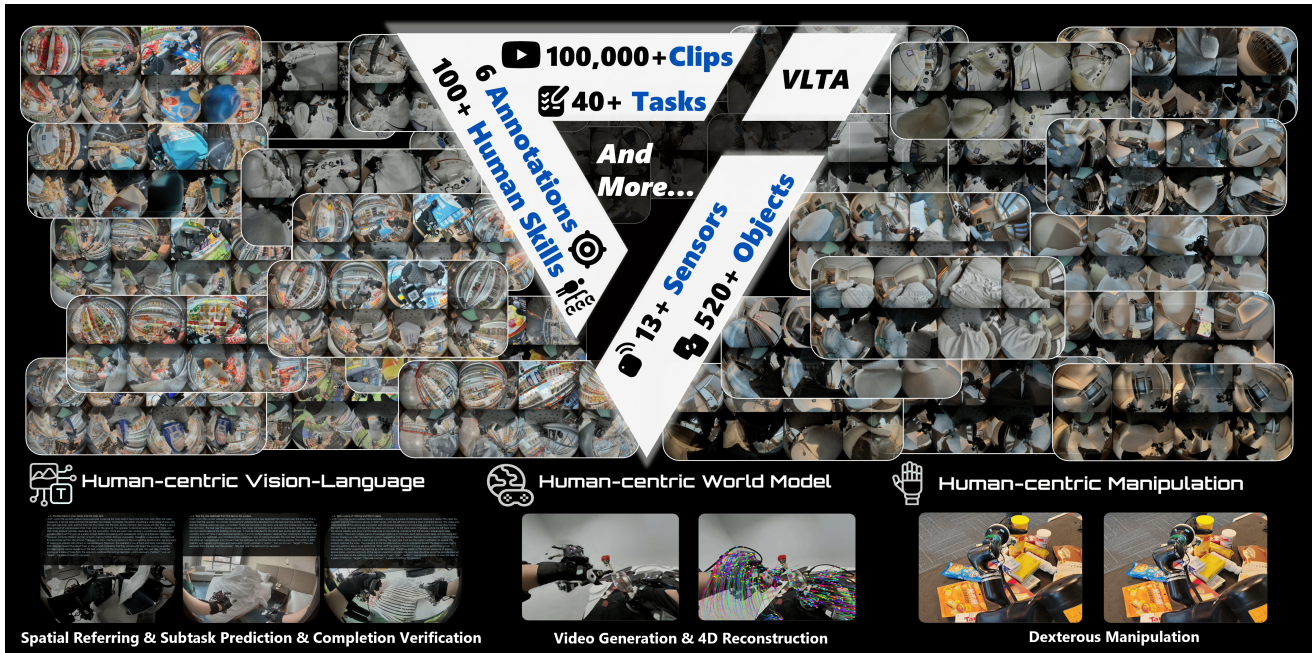


Figure 1. Our World In Your Hands (WiYH) ecosystem is built on top of a large-scale self-collected dataset in real-world human environments. It captures human subjects performing over 40 distinct tasks across a wide variety of scenarios. The dataset provides rich RGB video streams, along with comprehensive motion ground-truth encompassing more than 100 human skills. In addition to sensor and action data, it includes task annotations, depth information, and other annotations. This rich multimodal collection makes WiYH an excellent resource for research in spatial intelligence and Vision-Language-Action (VLA) learning.

Abstract

Large-scale pre-training is fundamental for generalization in language and vision models, but data for dexterous hand manipulation remains limited in scale and diversity, hindering policy generalization. Limited scenario diversity, misaligned modalities, and insufficient benchmarking constrain current human manipulation datasets. To address these gaps, we introduce World In Your Hands (WiYH), a large-scale open-source ecosystem for human-centric manipulation learning. WiYH includes (1) the Oracle Suite, a wearable data collection kit with an auto-

labeling pipeline for accurate motion capture; (2) the WiYH Dataset, featuring over 1,000 hours of multi-modal manipulation data across hundreds of skills in diverse real-world scenarios; and (3) extensive annotations and benchmarks supporting tasks from perception to action. Furthermore, experiments based on the WiYH ecosystem show that integrating WiYH’s human-centric data significantly enhances the generalization and robustness of dexterous hand policies in tabletop manipulation tasks. We believe that World In Your Hands will bring new insights into human-centric data collection and policy learning to the community.

1. Introduction

Large-scale pre-training has been established as a cornerstone for achieving generalization in Large Language Models [1, 8, 12, 41, 51], Vision-Language Models [2, 28–30, 36] and Vision-Language-Action Models [6, 7, 25, 47, 52, 55]. However, datasets for dexterous hand manipulation remain far smaller and less diverse than language datasets, limiting progress in learning robust manipulation policies.

To address the problem of data scarcity, human-centric data collection and learning have attracted growing interest [20, 23, 37, 53, 54]. Some approaches [4, 11, 27] capture human hand data during object manipulation using devices such as VR systems and smart glasses, while others [15, 17, 43, 49] leverage foundation models to extract human actions from unlabeled videos of human manipulation available on the internet.

Despite these advances, current human manipulation datasets still face three major limitations, as shown in Table 1 that hinder their usefulness for dexterous manipulation research: (1) **Limited Scenario Diversity**: Many datasets are collected in constrained laboratory environments, lacking the diversity and complexity of real-world settings. (2) **Inadequate Alignment**: Existing collections often lack one or more key modalities, such as the absence of fine-grained language instructions, precise 3D hand poses, or object poses, resulting in misalignment across vision, language, and action. (3) **Insufficient Benchmarking**: Most datasets do not support comprehensive evaluation benchmarks that span the entire pipeline of dexterous manipulation, including scene perception, task planning, and action.

To bridge this gap and investigate in-depth how human-centric data can advance dexterous manipulation, we introduce World In Your Hands (WiYH), a large-scale open-source ecosystem for learning human-centric manipulation in the wild, as shown in Figure 1. Specifically, the WiYH ecosystem comprises three core components:

- **The Oracle Suite and Auto-labeling Pipeline**. We introduce a lightweight and flexible wearable data collection kit, the Oracle Suite, designed to capture data without impeding the operator’s natural movements. An integrated auto-labeling pipeline enables markerless self-localization and centimeter-level motion accuracy without requiring external third-person tracking.
- **The WiYH Dataset: A Large-Scale Multi-modal Human-centric Dataset**. We present the WiYH dataset, a large-scale multi-modal resource comprising over 1,000 hours of manipulation sequences across hundreds of skills, captured in 10 diverse industrial and daily-life scenarios such as factories, supermarkets, hotels, and restaurants. The dataset includes rich sensory streams: multi-view images, camera calibration parameters, depth maps, 3D hand poses, and 6D wrist trajectories.
- **Diverse Annotations and Comprehensive Bench-**

marks. Building upon the WiYH dataset, we provide extensive annotations, including approximately 400 hours of atomic-level action instructions and 100k instances of vision-language data for task reasoning, affordance understanding, and object localization. These annotations support a comprehensive set of benchmarks—spanning visual language understanding, world model evaluation, and vision-language-action tasks—designed to assess capabilities from scene perception to embodied operation holistically.

Based on the WiYH ecosystem, we study how human-centric data empowers dexterous manipulation learning in tabletop manipulation tasks. We train models on mixtures of Oracle Suite demonstrations and other manipulation data and evaluate the task success rate across varied environments and object layouts. Our experiments demonstrate that human-centric data substantially improves the generalization and robustness of dexterous hand policies.

[Limitation]. All manipulation tasks are evaluated in real-world environments. To increase accessibility and reproducibility, we are developing high-fidelity simulation environments and plan to release them in a future version of the dataset and benchmarks.

2. World In Your Hands Ecosystem

2.1. Oracle Suite: Human-centric Data Collection Suite

To enable large-scale, high-fidelity, human-centric multi-modal data acquisition, we developed **Oracle Suite**, a low-cost wearable data collection system designed for human-centric embodied AI research. Specifically, as shown in Figure 2, Oracle Suite comprises a hardware system for acquiring multi-view RGB, IMU-based localization, and tactile information, alongside an autolabeling module that achieves high-precision motion capture through the fusion of IR, RGB, and IMU localization.

Hardware System Overview. Oracle Suite adopts a modular architecture integrating three primary hardware components: H-HPVHive, H-Gloves, and H-Backpack. This modular design enables flexible deployment across diverse environments, without being restricted to controlled indoor labs.

The Oracle Suite introduces major optimizations in ergonomics, sensing, and reliability:

- **H-FPVHive**: It supports chest-mounted configuration, and integrates two fisheye cameras, two pinhole cameras, and four infrared lenses. All cameras are hardware synchronized. The infrared lenses are used for better locating the relative poses of H-Gloves.
- **H-Gloves**: Each glove contains 6 IMUs, 5 pressure sensors, and an on-board MCU. The gloves can capture the hand motions and tactile. Moreover, it also contains 3

Table 1. **Comparison to existing datasets.** WiYH is characterized by two key distinctions: (1) Its entire 1000 hours of data were collected in the wild, with the tasks performed by skilled practitioners, thereby capturing the most authentic decision-making processes and actions; (2) Despite the significant challenge of annotating such a diverse, real-world collection, WiYH provides comprehensive annotations, including motion ground truth, depth, masks, task/sub-task labels, and chain-of-thought (CoT) reasoning, etc.

Dataset	Hours	Clips	Wild	Skills	Cam. Calib	RGB	Tactile	Action	Depth	Mask	Instruct.	Reason
Ego4D [15]	3,670	-	✓	✓	✗	✓	✗	2D	✗	✗	✓	✓
HOI4D [33]	44.4	4k	✓	✓	✓	✓	✗	2D	✓	✓	✗	✗
HoloAssist [45]	166	2.22k	✗	✗	✗	✓	✗	-	✓	✗	✓	✓
Ego-Exo4D [16]	1,286	5.04k	✓	✓	✓	✓	✗	✗	✗	✓	✓	✓
CaptainCook4D [35]	94.5	384	✓	✓	✗	✓	✗	✗	✓	✗	✓	✓
HOT3D [4]	13.9	425	✗	✗	✓	✓	✗	3D	✗	✗	✗	✗
HO-Cap [42]	-	64	✗	✗	✓	✓	✗	3D	✓	✓	✗	✗
Ego-ViD-5M [46]	-	5M	✓	✗	✓	✓	✗	✗	✗	✗	✓	✗
EgoDex [19]	829	338k	✗	✓	✗	✓	✗	3D	✗	✓	✓	✗
WiYH (Ours)	1045	125.4k	✓	✓	✓	✓	✓	3D	✓	✓	✓	✓

Oracle Suite: Human-centric Data Collection Suite



Figure 2. **Oracle Suite: Human-centric Data Collection Suite.** It is primarily composed of three integrated components: (1) H-FPVHive: A first-person perception suite equipped with multiple cameras of different modalities to comprehensively record the operator’s environmental context. (2) H-Glove: A hand motion capture and tactile perception module. It integrates motion capture gloves, tactile sensors, and visual trackers. The H-Glove is synchronized with the H-FPVHive, enabling precise action localization and capture in unstructured, real-world settings. (3) H-Backpack: A power supply and data storage unit.

fisheye cameras for visual tracking and observation.

- **H-Backpack:** It provides data storage, computation, and power supply. The computation is hosted by NVIDIA Orin.

Autolabeling Pipeline. As shown in the right part of Figure 2, the Autolabeling Pipeline comprises both online and offline algorithms. It fuses multi-modal sensor data (IR + IMU + RGB) to ensure positioning accuracy in in-the-wild scenarios. Specifically, the online localization module performs lightweight coarse positioning using visual-inertial odometry (VIO) algorithms and IR detection, while the offline stage refines these coarse estimates through visual Structure-from-Motion (SfM) algorithms. The pipeline ultimately outputs centimeter-level 6D poses for both wrists.

Data Production Efficiency. The Oracle Suite pipeline fol-

lows a *collection–annotation–inspection–archiving* workflow for scalable data production. A single collector operating 5 hours per day generates approximately 1.8 TB of valid multimodal data. At scale, 100 collectors over 30 days yield roughly 5.4 PB of raw data (stored in cloud repositories). Efficiency is further improved through standardized capture protocols and automated cloud-based annotation.

2.2. Data Annotation Pipeline

Data collection: Practitioners wore the Oracle Suite in each scene to record natural manipulation behavior. Each recording session lasted approximately 10 minutes and included start and end event markers. The collected signals comprise tactile signals from pressure sensors, binocular fisheye images from the left and right wrist mounts, first-person binoc-

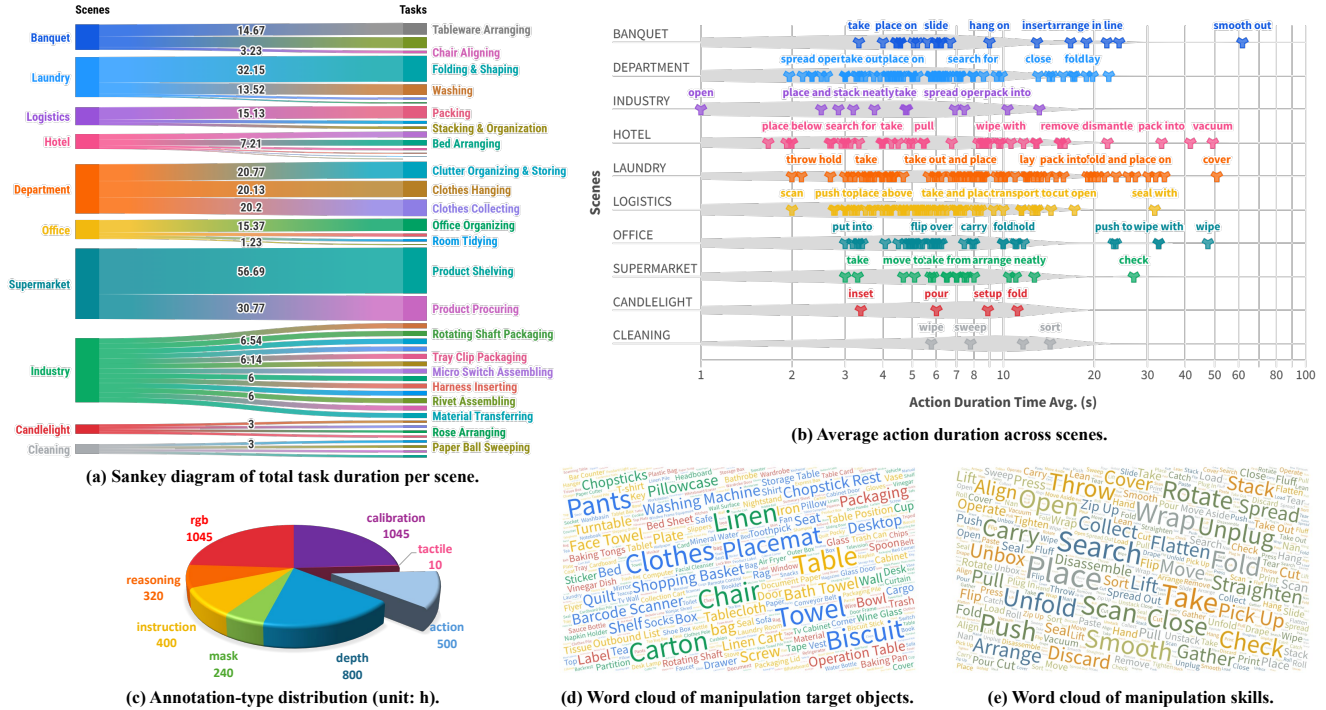


Figure 3. Overview of dataset statistics, including task–scene relationships, action durations, annotation distributions, and word clouds of manipulation target objects and skills. The dataset spans a wide spectrum of real-world scenarios, from industrial to daily-life (e.g., factories, hotels, apartments, supermarkets). For each scenario, it provides task and subtask annotations crucial for instruction-action alignment and task decomposition in VLA models. The chart presents multi-dimensional statistics of these annotations.

ular fisheye images, left-hand and right-hand IMU localization data, and the corresponding camera calibration parameters. Samples of data annotations are shown in Figure 4.

Data annotation: The annotation pipeline comprises three parts: subtask (atomic task) annotation, perception annotation, and vision-language annotation.

Subtask annotation: To construct a large-scale, high-quality set of atomic tasks, we designed a four-stage hybrid annotation pipeline consisting of data processing, task definition, annotation consolidation, and post-processing:

(1) **Data processing:** First-person fisheye videos are segmented into 30-second clips, which serve as the basic units for semantic annotation by the video-language module;

(2) **Task definition (manual annotation):** The video-language module parses hierarchical operational semantics from the first-person videos and hierarchically decomposes an operation sequence into high-level tasks and atomic subtask units. Each task unit contains a preset action described in natural language and a manually annotated target object.

(3) **Data checking (manual review):** Outputs from the video-language module are subject to iterative manual review; any incorrect annotations are reprocessed before proceeding to the consolidation stage.

(4) **Post-processing:** Annotated preset-action and target-object names are assembled into complete operation instructions and are further augmented using a large language model (LLM). After subtask annotation, the raw data are organized into a hierarchical format of tasks composed of multiple atomic subtasks.

Perception annotation: To provide richer perceptual information, we pre-annotated scene elements using visual foundation models and then performed manual selection and correction. The resulting perception annotations include:

(1) **Segmentation masks:** instance masks are generated by applying SAM to human-provided prompt points;

(2) **Depth maps:** scene depth is estimated from first-person binocular images using the FoundationStereo model.

Vision-language annotation: The vision-language annotations were produced through manual curation and comprise the following tasks:

(1) **Spatial Referring:** For each subtask, we extract a key frame near the action start that contains the operator’s object of attention and in which the target object is not occluded by the hand, body, or other objects. Based on the subtask’s target object, spatial relational terms are added to uniquely refer to a single target region in the image.

(2) **Subtask Prediction:** We select tasks that contain 4–5

subtasks. The next subtask following the current one is used as the correct option. Nine incorrect options are generated by combining scene object information and the task’s pre-set actions; annotators then select the three incorrect options that are the most logically plausible. Additionally, Qwen-2.5VL-72B was used to generate auxiliary “thinking” data for next-action prediction, which were subsequently corrected by human annotators;

(3) **Completion Verification:** We select tasks containing 4-5 subtasks and randomly trim the tail of the video by 20%, 25%, 30%, or 35% of frames. The task description and the truncated video are provided as input, and human annotators label whether the video depicts a completed task.

Through the above procedures, we obtain rich annotations covering scene understanding and task planning, which constitute the foundation of a unified benchmark.

2.3. Data Statistics

Figure 3 summarizes key statistics of our WiYH dataset. We first analyze the distribution of tasks across scenes. As shown in Figure 3(a), WiYH contains a diverse set of daily environments, including banquet, laundry, logistics, hotel, department, office, supermarket, industry, cleaning, and candlelight settings. The Sankey diagram illustrates the total accumulated duration of each task within its corresponding scene.

Scenes such as supermarkets and laundry include long-horizon activities with substantial execution time, while hotels and candlelight contain shorter but highly structured routines. This diversity in task–scene composition highlights the wide operational range covered by WiYH. Action-level temporal characteristics are shown in Figure 3(b). For each scene, we compute the average execution duration of fine-grained actions. The dataset exhibits substantial variation across action categories, from short, instantaneous operations such as wipe and insert, to long-horizon manipulation such as smooth out or foldlay. These temporal differences reflect the heterogeneous complexity of real-world household and industrial workflows.

Figure 3(c) reports the distribution of annotation types. WiYH includes rich multimodal and task-level supervision, consisting of RGB, depth, action, instruction, reasoning, mask, tactile, and calibration annotations. Among them, RGB and calibration frames appear most frequently, while reasoning and tactile annotations, though smaller in quantity, provide high-level semantic cues crucial for complex manipulation and planning tasks.

To better understand the manipulation space in WiYH, Figure 3(d–e) visualizes word clouds of the annotated target objects and skills. The dataset covers a broad range of manipulable objects—including clothes, linens, cartons, cups, and tableware—spanning deformable, rigid, and articulated categories. Likewise, the skill vocabulary encompasses di-

verse manipulation primitives such as take, place, rotate, unfold, align, push, and search, representing both low-level motor actions and higher-level task strategies. These distributions further demonstrate that WiYH captures a wide spectrum of real-world manipulation behaviors.

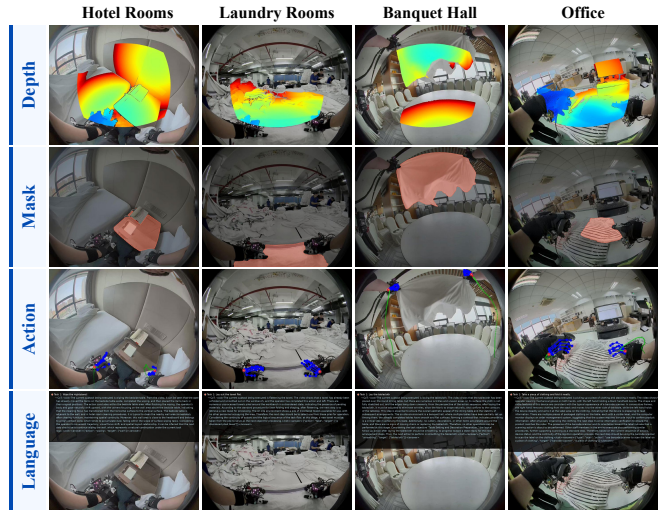


Figure 4. **Data annotation samples cross different scenes.** The example of human video annotations, including depth, mask, action and task descriptions in four scenarios.

3. Benchmark and Applications

3.1. Human-centric Vision-Language (HVL)

In this section, we construct three evaluation tasks based on the vision-language annotations introduced in Section 2. These tasks are designed to evaluate whether existing Multimodal Large Language Models (MLLMs) can achieve a genuine understanding of human-centric manipulation tasks in highly generalized in-the-wild environments.

We define the following three evaluation tasks and test several closed-source and open-source MLLMs, including GPT-4o [22], Doubao-seed [3], and Qwen [51]. Detailed experimental setups and data statistics are provided in the supplementary material. (1) **Spatial Referring (SR):** Given a human manipulation image and a description of the spatial relationships among multiple objects in the scene, the model is required to output the pixel coordinates of a specified region. Performance is measured by the probability that the predicted point lies within the target area. (2) **Sub-task Prediction (SP):** Given a piece of human manipulation video, the current task description, and four candidate options for the next action, the model must select the correct subsequent action. (3) **Completion Verification (CV):** Given a piece of human manipulation video and the current task description, the model needs to determine whether the task has been completed.

Table 2. Comparison of VLMs on spatial reasoning tasks.

Model	SR (%)	SP (%)	CV (%)
GPT-4o [34]	10.04	73.40	51.18
Qwen3-VL-Plus [39]	46.53	71.75	55.89
Doubao-Seed-1.6-Vision [9]	39.83	76.84	51.96
Qwen3-VL-4B-Instruct [40]	25.58	69.21	56.73

Table 3. Comparison of consistency, smoothness, dynamic, and quality metrics under different conditions .

Metric	CogVideo [18]		DynamiCrafter [48]	
	w/o WiYH	w/ WiYH	w/o WiYH	w/ WiYH
Consistency \uparrow	80.6	88.2 (+7.6)	85.3	91.5 (+6.2)
Smoothness \uparrow	93.5	98.4 (+4.9)	97.4	98.6 (+1.2)
Dynamic \uparrow	62.9	78.5 (+15.6)	74.8	89.6 (+14.8)
Quality \uparrow	60.1	67.6 (+7.5)	63.5	70.6 (+7.1)

As shown in Table 2, Qwen3-VL-Plus, which was pre-trained on spatial understanding data, achieves the best performance on the Spatial Referring task. However, scores of all MLLMs are below 0.5, indicating that current MLLMs still lack sufficient capability in interpreting fine-grained spatial relationships in manipulation scenarios. On the Completion Verification task, all models perform slightly above 0.5, suggesting that their ability to accurately judge task completion in such contexts remains limited. These experimental results collectively demonstrate that general-purpose, vanilla VLLMs still fall short in embodied tasks. Our WiYH dataset, with its rich annotations of human activities and spatial relationships, presents a promising foundation for future embodied pre-training.

3.2. Human-centric World Model (HWM)

3.2.1. Language-conditioned Video Generation

This section evaluates the contribution of our proposed WiYH dataset to enhancing video generation performance in human-centric manipulation tasks. We fine-tuned two baseline models, CogVideo [18] and DynamiCrafter [48], initialized with their original weights, using WiYH under the image-and-text-to-video setting. During fine-tuning, all input videos were resized to 480p resolution.

As shown in Figure 5, models fine-tuned with WiYH generate egocentric videos with improved spatial and temporal coherence, as well as stronger alignment with both the input image and action instructions. For example, in the “Wipe the cabinet” task, the cabinet’s orientation and the towel’s color are reproduced more accurately. In contrast, videos generated by non-fine-tuned models exhibit noticeable object fragmentation and distortion, along with discontinuous and physically implausible hand-object interactions. Notably, after fine-tuning, the complex motions of non-rigid objects in the generated videos appear more re-

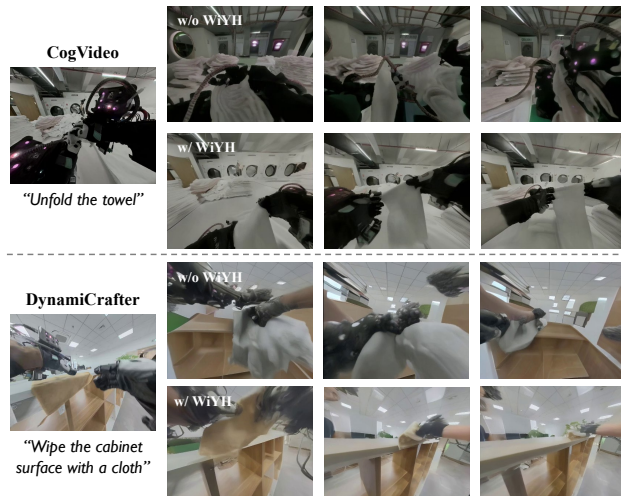


Figure 5. **Language-conditioned Video Generation.** When provided with language instructions, two baseline video prediction methods exhibited significant hallucinations without WiYH fine-tuning. However, after fine-tuning on our dataset, they demonstrated a markedly enhanced ability to imagine future states.

alistic and natural. These improvements demonstrate that WiYH substantially enhances a model’s ability to capture real-world dynamics.

Quantitative results are summarized in Table 3. We use four metrics from VBench [21]—consistency, smoothness, dynamic (motion intensity), and quality—to assess motion plausibility, temporal coherence, and visual fidelity. After fine-tuning with the WiYH dataset, both baseline models show clear improvements across all metrics, with the most significant gains observed in motion intensity and temporal consistency.

3.2.2. Gaussian Splatting 4D Reconstruction

This subsection evaluates the dataset’s utility for supervised end-to-end 4D reconstruction using Gaussian Splatting (GS). By providing high-quality RGB images, depth maps, and camera poses, WiYH supports shape and motion modeling for dynamic scenes. We extracted geometry using MegaSAM [32], tracked pixel trajectories of dynamic objects with TAPIR [13], and performed scene reconstruction with Shape of Motion [44]. The successful application of our dataset in spatial perception tasks like 4D Gaussian Splatting (4DGS) demonstrates the critical role of its rich annotations, particularly depth information, in enhancing spatial understanding and representation.

As shown in Table 4, photometric metrics remain relatively consistent, whereas geometric metrics vary notably across tasks. These differences highlight the inherent challenges in reconstructing dynamic scenes, where accurate geometry prediction is particularly complex in motion-rich environments. This observation suggests promising direc-

Table 4. Comparison of photometric and geometric metrics for different tasks.

Scene	Task	Photometry			Geometry	
		PSNR \uparrow	SSIM \uparrow	LPIPS \downarrow	A.R. \downarrow	$\delta_1\uparrow$
1	Pouring Wine	20.15	0.815	0.206	1.04	52.01
2	Packing Clothes	20.02	0.656	0.423	2.89	17.83
3	Packing Cargo	18.83	0.749	0.552	3.52	13.79

tions for future research in 4D reconstruction for robotic manipulation, particularly methods that improve geometric understanding in complex dynamic scenes.

Figure 6 presents the 4D reconstruction results at various time steps, showcasing the dataset’s potential for dynamic scene modeling. By capturing high-quality dynamic scenes, WiYH can help leverage Gaussian Splatting (GS) as an effective 3D tokenizer, advance spatial understanding, and enrich Real2Sim pipelines.

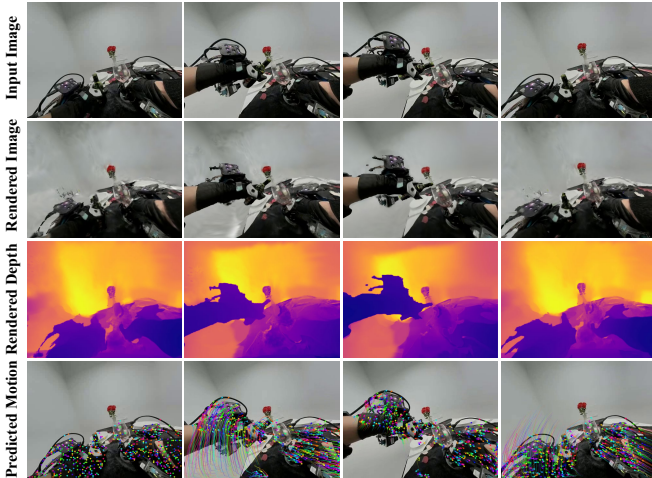


Figure 6. **4D Reconstruction Result.** For the pouring wine task, we present the 4DGS reconstruction results across multiple time-stamps. The visualizations include the rendered image, estimated depth map, and predicted 4D motion field. The results demonstrate that our WiYH dataset enables clean and accurate 4D reconstruction, even in challenging, dynamic action scenarios.

3.3. Human-centric VLA Training (HVT)

In this section, we evaluate several Vision-Language-Action (VLA) algorithms trained on the WiYH dataset to explore whether its visual-action-language tri-modal support enables effective training of vision-language-action-aligned manipulation policies.

Specifically, we use GR00T [5] and OpenVLA-OFT [26] as baseline algorithms, training each to predict the future 1.6-second motion trajectory (16 points at 10 Hz) of the human wrist from the dataset. We sample 10% of the data from each scenario for training and assemble a test set

Table 5. VLA performance with different training steps.

Model	Mean Error (cm)		
	0 Steps	15k Steps	30k Steps
OpenVLA-OFT [26]	4.75	1.28	1.12
GR00T [5]	4.54	1.31	1.07

of 400 non-overlapping episodes. Each baseline model is trained for 30,000 steps with a total batch size of 128 on 8 NVIDIA A100 GPUs.

As shown in Table 5, training with human-centric data consistently reduces the error in tracking the ground-truth trajectories on the test set across both mainstream VLA frameworks. These results demonstrate WiYH’s effectiveness for training VLA algorithms. We believe the WiYH dataset can serve as a foundational resource for validating scaling laws in human-centric VLA pre-training.

4. Cross-Embodiment Analysis

In this section, we conduct co-training experiments using cross-embodiment data to investigate the effectiveness of the human video data.

4.1. Implementation Details

We set up two scenarios: a single-object scene and a multi-object cluttered scene. In this experiment, we employ a co-training policy using data collected by an improved version of DexUMI [50] and from Human Video demonstrations. Figure 8 shows representative scene examples and the data collection setup. For UMI, data collection always started from a limited number of initial poses. The improved UMI system is capable of capturing trajectories with millimeter-level accuracy and was exclusively used to collect high-precision manipulation data in the single-object scene, resulting in fine-grained motion trajectories. In contrast, Human Video contains only manipulation sequences from multi-object cluttered scenes, providing data that spans a larger action space, exhibits a broader distribution of motions, and covers a greater diversity of object observations.

4.2. Results and In-depth Discussion

In the single-object scenario, the robot arm begins execution from a random initial pose during testing, which differs from the initial pose used in the UMI dataset. In the multi-object cluttered scenario, we primarily evaluate the performance of the co-training strategy under conditions of varying scene height, changes in the target object’s pose, and increased occlusion. The configurations of these test scenarios and qualitative experimental results are illustrated in Figure 7.

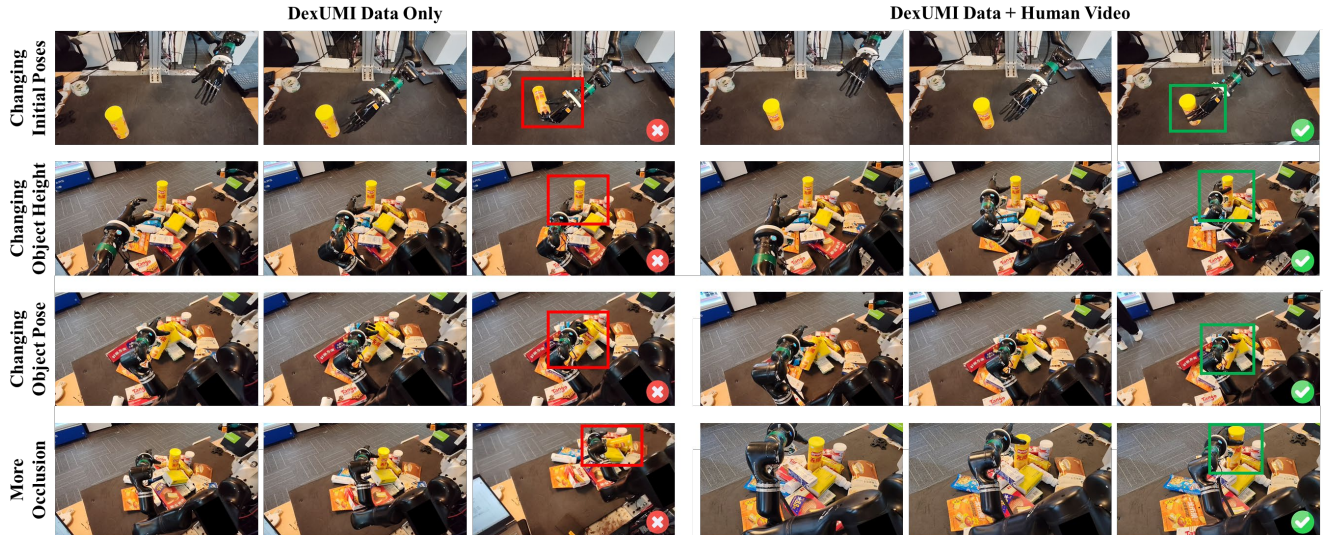


Figure 7. **Real-robot manipulation experiments.** We present the comparison of manipulation policy performance under four novel task settings, where the policies are trained either exclusively on data collected by UMI or co-trained using both UMI data and annotated human demonstration videos (WiYH).



Figure 8. **Comparison of data collection.** UMI collects single-object manipulation data starting from a limited set of initial poses, whereas Human Video contains data from more complex scenes and covers a broader action space.

Quantitative results are summarized in Table 6. (1) In the single-object scenario, co-training the policy with both UMI data and Human Video data leads to an improvement in the success rate of more than 13%. Although the motion precision in the human data is limited, its diverse action distribution enhances the policy’s generalization capability to unseen initial states. (2) Policies trained solely on UMI data exhibit almost no generalization ability in complex scenarios; however, after co-training with human data, the SR increases by 52%. This demonstrates that incorporating human data significantly improves the policy’s ability to interpret complex scenes. Therefore, the co-training approach effectively introduces both the action domain and observation domain of human data into the robot dataset, thereby enhancing the generalization capability of the learned policy.

Table 6. A comparison of results on two manipulation scenarios trained with data from different sources is presented. The datasets include data collected by UMI and human demonstration videos (WiYH). And the success rate (SR) was reported.

Scenario	Data Sources and Amounts		SR (%)
	UMI (clips)	Human Video (clips)	
Single-object Scene	200	0	20
	200	800	23.3 (+3.3)
	500	0	43.3
	500	800	56.7 (+13.4)
Cluttered Scene	200	0	0.0
	200	800	32.0 (+32.0)
	500	0	8.0
	500	800	60.0 (+52.0)

5. Conclusion

This paper presents the WiYH ecosystem, a cornerstone for embodied intelligence research in real-world environments. We make three key contributions: the Oracle Suite, a wearable system enabling in-the-wild data capture with integrated markerless auto-labeling; the large-scale WiYH Dataset, offering diverse, skilled human manipulation sequences with rich multi-modal streams; and a suite of Comprehensive Benchmarks, supported by extensive atomic-action and vision-language annotations, for holistic evaluation from perception to physical interaction. Our benchmarks reveal that current models still lack the fine-grained spatial and causal reasoning required for robust embodied operation. The WiYH dataset, with its unique scale, and rich annotations, is designed to bridge this gap. We believe this work provides an essential foundation for developing more capable and generalizable embodied agents.

References

- [1] Josh Achiam, Steven Adler, Sandhini Agarwal, Lama Ahmad, Ilge Akkaya, Florencia Leoni Aleman, Diogo Almeida, Janko Altenschmidt, Sam Altman, Shyamal Anadkat, et al. Gpt-4 technical report. *arXiv preprint arXiv:2303.08774*, 2023. 2
- [2] Jean-Baptiste Alayrac, Jeff Donahue, Pauline Luc, Antoine Miech, Iain Barr, Yana Hasson, Karel Lenc, Arthur Mensch, Katherine Millican, Malcolm Reynolds, et al. Flamingo: a visual language model for few-shot learning. *Advances in neural information processing systems*, 35:23716–23736, 2022. 2
- [3] Ye Bai, Haonan Chen, Jitong Chen, Zhuo Chen, Yi Deng, Xiaohong Dong, Lamtharn Hantrakul, Weituo Hao, Qingqing Huang, Zhongyi Huang, et al. Seed-music: A unified framework for high quality and controlled music generation. *arXiv preprint arXiv:2409.09214*, 2024. 5
- [4] Prithviraj Banerjee, Sindi Shkodrani, Pierre Moulon, Shreyas Hampali, Shangchen Han, Fan Zhang, Linguang Zhang, Jade Fountain, Edward Miller, Selen Basol, et al. Hot3d: Hand and object tracking in 3d from egocentric multi-view videos. In *Proceedings of the Computer Vision and Pattern Recognition Conference*, pages 7061–7071, 2025. 2, 3
- [5] Johan Bjorck, Fernando Castañeda, Nikita Cherniadev, Xingye Da, Runyu Ding, Linxi Fan, Yu Fang, Dieter Fox, Fengyuan Hu, Spencer Huang, et al. Gr00t n1: An open foundation model for generalist humanoid robots. *arXiv preprint arXiv:2503.14734*, 2025. 7
- [6] Kevin Black, Noah Brown, Danny Driess, Adnan Esmail, Michael Equi, Chelsea Finn, Niccolo Fusai, Lachy Groom, Karol Hausman, Brian Ichter, et al. π 0: A vision-language-action flow model for general robot control. corr, abs/2410.24164, 2024. doi: 10.48550. *arXiv preprint ARXIV.2410.24164*. 2
- [7] Anthony Brohan, Noah Brown, Justice Carbajal, Yevgen Chebotar, Joseph Dabis, Chelsea Finn, Keerthana Gopalakrishnan, Karol Hausman, Alex Herzog, Jasmine Hsu, et al. Rt-1: Robotics transformer for real-world control at scale. *arXiv preprint arXiv:2212.06817*, 2022. 2
- [8] Tom Brown, Benjamin Mann, Nick Ryder, Melanie Subbiah, Jared D Kaplan, Prafulla Dhariwal, Arvind Neelakantan, Pranav Shyam, Girish Sastry, Amanda Askell, et al. Language models are few-shot learners. *Advances in neural information processing systems*, 33:1877–1901, 2020. 2
- [9] ByteDance Doubao Team. Doubao seed 1.6-vision: A hybrid-training vision-language model, 2024. Accessed: 2025-11-14. 6
- [10] Mathilde Caron, Hugo Touvron, Ishan Misra, Hervé Jégou, Julien Mairal, Piotr Bojanowski, and Armand Joulin. Emerging properties in self-supervised vision transformers. In *Proceedings of the IEEE/CVF international conference on computer vision*, pages 9650–9660, 2021. 2
- [11] Yu-Wei Chao, Wei Yang, Yu Xiang, Pavlo Molchanov, Ankur Handa, Jonathan Tremblay, Yashraj S Narang, Karl Van Wyk, Umar Iqbal, Stan Birchfield, et al. Dexycb: A benchmark for capturing hand grasping of objects. In *Proceedings of the IEEE/CVF conference on computer vision and pattern recognition*, pages 9044–9053, 2021. 2
- [12] Aakanksha Chowdhery, Sharan Narang, Jacob Devlin, Maarten Bosma, Gaurav Mishra, Adam Roberts, Paul Barham, Hyung Won Chung, Charles Sutton, Sebastian Gehrmann, et al. Palm: Scaling language modeling with pathways. *Journal of Machine Learning Research*, 24(240): 1–113, 2023. 2
- [13] Carl Doersch, Yi Yang, Mel Vecerik, Dilara Gokay, Ankush Gupta, Yusuf Aytar, Joao Carreira, and Andrew Zisserman. Tapir: Tracking any point with per-frame initialization and temporal refinement. In *Proceedings of the IEEE/CVF International Conference on Computer Vision*, pages 10061–10072, 2023. 6
- [14] Yuming Fang, Hanwei Zhu, Yan Zeng, Kede Ma, and Zhou Wang. Perceptual quality assessment of smartphone photography. In *Proceedings of the IEEE/CVF conference on computer vision and pattern recognition*, pages 3677–3686, 2020. 2
- [15] Kristen Grauman, Andrew Westbury, Eugene Byrne, Zachary Chavis, Antonino Furnari, Rohit Girdhar, Jackson Hamburger, Hao Jiang, Miao Liu, Xingyu Liu, et al. Ego4d: Around the world in 3,000 hours of egocentric video. In *Proceedings of the IEEE/CVF conference on computer vision and pattern recognition*, pages 18995–19012, 2022. 2, 3
- [16] Kristen Grauman, Andrew Westbury, Lorenzo Torresani, Kris Kitani, Jitendra Malik, Triantafyllos Afouras, Kumar Ashutosh, Vijay Baiyya, Siddhant Bansal, Bikram Boote, et al. Ego-exo4d: Understanding skilled human activity from first-and third-person perspectives. In *Proceedings of the IEEE/CVF Conference on Computer Vision and Pattern Recognition*, pages 19383–19400, 2024. 3
- [17] Yuzhe He, Shuang Liang, Xiaofei Rui, Chengying Cai, and Guowei Wan. EgoVn: Achieving precise ego-localization using lightweight vectorized maps. In *2024 IEEE/RSJ International Conference on Intelligent Robots and Systems (IROS)*, pages 12248–12255. IEEE, 2024. 2
- [18] Wenyi Hong, Ming Ding, Wendi Zheng, Xinghan Liu, and Jie Tang. Cogvideo: Large-scale pretraining for text-to-video generation via transformers. In *The Eleventh International Conference on Learning Representations*, 2022. 6, 2
- [19] Ryan Hoque, Peide Huang, David J Yoon, Mouli Sivapurapu, and Jian Zhang. EgoDex: Learning dexterous manipulation from large-scale egocentric video. *arXiv preprint arXiv:2505.11709*, 2025. 3
- [20] Jhen Hsieh, Kuan-Hsun Tu, Kuo-Han Hung, and Tsung-Wei Ke. Dexman: Learning bimanual dexterous manipulation from human and generated videos. *arXiv preprint arXiv:2510.08475*, 2025. 2
- [21] Ziqi Huang, Yinan He, Jiashuo Yu, Fan Zhang, Chenyang Si, Yuming Jiang, Yuanhan Zhang, Tianxing Wu, Qingyang Jin, Nattapol Chanpaisit, et al. Vbench: Comprehensive benchmark suite for video generative models. In *Proceedings of the IEEE/CVF Conference on Computer Vision and Pattern Recognition*, pages 21807–21818, 2024. 6, 2

- [22] Aaron Hurst, Adam Lerer, Adam P Goucher, Adam Perelman, Aditya Ramesh, Aidan Clark, AJ Ostrow, Akila Welihinda, Alan Hayes, Alec Radford, et al. Gpt-4o system card. *arXiv preprint arXiv:2410.21276*, 2024. 5
- [23] Simar Kareer, Dhruv Patel, Ryan Punamiya, Pranay Mathur, Shuo Cheng, Chen Wang, Judy Hoffman, and Danfei Xu. Egomimic: Scaling imitation learning via egocentric video. In *2025 IEEE International Conference on Robotics and Automation (ICRA)*, pages 13226–13233. IEEE, 2025. 2
- [24] Junjie Ke, Qifei Wang, Yilin Wang, Peyman Milanfar, and Feng Yang. Musiq: Multi-scale image quality transformer. In *Proceedings of the IEEE/CVF international conference on computer vision*, pages 5148–5157, 2021. 2
- [25] Moo Jin Kim, Karl Pertsch, Siddharth Karamcheti, Ted Xiao, Ashwin Balakrishna, Suraj Nair, Rafael Rafailov, Ethan Foster, Grace Lam, Pannag Sanketi, et al. Openvla: An open-source vision-language-action model. *arXiv preprint arXiv:2406.09246*, 2024. 2
- [26] Moo Jin Kim, Chelsea Finn, and Percy Liang. Fine-tuning vision-language-action models: Optimizing speed and success. *arXiv preprint arXiv:2502.19645*, 2025. 7
- [27] Taein Kwon, Bugra Tekin, Jan Stühmer, Federica Bogo, and Marc Pollefeys. H2o: Two hands manipulating objects for first person interaction recognition. In *Proceedings of the IEEE/CVF international conference on computer vision*, pages 10138–10148, 2021. 2
- [28] Feng Li, Renrui Zhang, Hao Zhang, Yuanhan Zhang, Bo Li, Wei Li, Zejun Ma, and Chunyuan Li. Llava-next-interleave: Tackling multi-image, video, and 3d in large multimodal models. *arXiv preprint arXiv:2407.07895*, 2024. 2
- [29] Junnan Li, Dongxu Li, Caiming Xiong, and Steven Hoi. Blip: Bootstrapping language-image pre-training for unified vision-language understanding and generation. In *International conference on machine learning*, pages 12888–12900. PMLR, 2022.
- [30] Junnan Li, Dongxu Li, Silvio Savarese, and Steven Hoi. Blip-2: Bootstrapping language-image pre-training with frozen image encoders and large language models. In *International conference on machine learning*, pages 19730–19742. PMLR, 2023. 2
- [31] Zhen Li, Zuo-Liang Zhu, Ling-Hao Han, Qibin Hou, Chun-Le Guo, and Ming-Ming Cheng. Amt: All-pairs multi-field transforms for efficient frame interpolation. In *Proceedings of the IEEE/CVF Conference on Computer Vision and Pattern Recognition*, pages 9801–9810, 2023. 2
- [32] Zhengqi Li, Richard Tucker, Forrester Cole, Qianqian Wang, Linyi Jin, Vickie Ye, Angjoo Kanazawa, Aleksander Holynski, and Noah Snavely. Megasam: Accurate, fast and robust structure and motion from casual dynamic videos. In *Proceedings of the Computer Vision and Pattern Recognition Conference*, pages 10486–10496, 2025. 6
- [33] Yunze Liu, Yun Liu, Che Jiang, Kangbo Lyu, Weikang Wan, Hao Shen, Boqiang Liang, Zhoujie Fu, He Wang, and Li Yi. Hoi4d: A 4d egocentric dataset for category-level human-object interaction. In *Proceedings of the IEEE/CVF Conference on Computer Vision and Pattern Recognition*, pages 21013–21022, 2022. 3
- [34] OpenAI. Gpt-4o: The omni model. Technical report, 2024. Accessed: 2025-11-14. 6
- [35] Rohith Peddi, Shivvrat Arya, Bharath Challa, Likhitha Palapothula, Akshay Vyas, Bhavya Gouripeddi, Qifan Zhang, Jikai Wang, Vasundhara Komaragiri, Eric Ragan, et al. Captaincook4d: A dataset for understanding errors in procedural activities. *Advances in Neural Information Processing Systems*, 37:135626–135679, 2024. 3
- [36] Alec Radford, Jong Wook Kim, Chris Hallacy, Aditya Ramesh, Gabriel Goh, Sandhini Agarwal, Girish Sastry, Amanda Askell, Pamela Mishkin, Jack Clark, et al. Learning transferable visual models from natural language supervision. In *International conference on machine learning*, pages 8748–8763. Pmlr, 2021. 2
- [37] Sandeep Routray, Hengkai Pan, Unnat Jain, Shikhar Bahl, and Deepak Pathak. Vipra: Video prediction for robot actions. *arXiv preprint arXiv:2511.07732*, 2025. 2
- [38] Zachary Teed and Jia Deng. Raft: Recurrent all-pairs field transforms for optical flow. In *European conference on computer vision*, pages 402–419. Springer, 2020. 2
- [39] Tongyi Lab, Alibaba Cloud. Qwen3-vl: Advancing vision-language understanding with scalable multimodal pretraining, 2025. Accessed: 2025-11-14. 6
- [40] Tongyi Lab, Alibaba Cloud. Qwen3-vl-4b-instruct: Instruction-tuned vision-language model, 2025. Model version: qwen3-vl-4b-instruct. Accessed: 2025-11-14. 6
- [41] Hugo Touvron, Thibaut Lavril, Gautier Izacard, Xavier Martinet, Marie-Anne Lachaux, Timothée Lacroix, Baptiste Rozière, Naman Goyal, Eric Hambro, Faisal Azhar, et al. Llama: Open and efficient foundation language models. *arXiv preprint arXiv:2302.13971*, 2023. 2
- [42] Jikai Wang, Qifan Zhang, Yu-Wei Chao, Bowen Wen, Xiaohu Guo, and Yu Xiang. Ho-cap: A capture system and dataset for 3d reconstruction and pose tracking of hand-object interaction. *arXiv preprint arXiv:2406.06843*, 2024. 3
- [43] Mengmeng Wang, Jiazheng Xing, and Yong Liu. Actionclip: A new paradigm for video action recognition. *arXiv preprint arXiv:2109.08472*, 2021. 2
- [44] Qianqian Wang, Vickie Ye, Hang Gao, Weijia Zeng, Jake Austin, Zhengqi Li, and Angjoo Kanazawa. Shape of motion: 4d reconstruction from a single video. In *Proceedings of the IEEE/CVF International Conference on Computer Vision*, pages 9660–9672, 2025. 6
- [45] Xin Wang, Taein Kwon, Mahdi Rad, Bowen Pan, Ishani Chakraborty, Sean Andrist, Dan Bohus, Ashley Feniello, Bugra Tekin, Felipe Vieira Frujeri, et al. Holoassist: an egocentric human interaction dataset for interactive ai assistants in the real world. In *Proceedings of the IEEE/CVF International Conference on Computer Vision*, pages 20270–20281, 2023. 3
- [46] Xiaofeng Wang, Kang Zhao, Feng Liu, Jiayu Wang, Guosheng Zhao, Xiaoyi Bao, Zheng Zhu, Yingya Zhang, and Xingang Wang. Egovid-5m: A large-scale video-action dataset for egocentric video generation. *arXiv preprint arXiv:2411.08380*, 2024. 3
- [47] Junjie Wen, Minjie Zhu, Yichen Zhu, Zhibin Tang, Jinming Li, Zhongyi Zhou, Chengmeng Li, Xiaoyu Liu, Yaxin Peng,

- Chaomin Shen, et al. Diffusion-vla: Generalizable and interpretable robot foundation model via self-generated reasoning. *arXiv preprint arXiv:2412.03293*, 2024. [2](#)
- [48] Jinbo Xing, Menghan Xia, Yong Zhang, Haoxin Chen, Wangbo Yu, Hanyuan Liu, Gongye Liu, Xintao Wang, Ying Shan, and Tien-Tsin Wong. Dynamicrafter: Animating open-domain images with video diffusion priors. In *European Conference on Computer Vision*, pages 399–417. Springer, 2024. [6](#), [2](#)
- [49] Hu Xu, Gargi Ghosh, Po-Yao Huang, Dmytro Okhonko, Armen Aghajanyan, Florian Metze, Luke Zettlemoyer, and Christoph Feichtenhofer. Videoclip: Contrastive pre-training for zero-shot video-text understanding. *arXiv preprint arXiv:2109.14084*, 2021. [2](#)
- [50] Mengda Xu, Han Zhang, Yifan Hou, Zhenjia Xu, Linxi Fan, Manuela Veloso, and Shuran Song. Dexumi: Using human hand as the universal manipulation interface for dexterous manipulation. *arXiv preprint arXiv:2505.21864*, 2025. [7](#)
- [51] An Yang, Anfeng Li, Baosong Yang, Beichen Zhang, Binyuan Hui, Bo Zheng, Bowen Yu, Chang Gao, Chengen Huang, Chenxu Lv, et al. Qwen3 technical report. *arXiv preprint arXiv:2505.09388*, 2025. [2](#), [5](#)
- [52] Zhongyi Zhou, Yichen Zhu, Junjie Wen, Chaomin Shen, and Yi Xu. Vision-language-action model with open-world embodied reasoning from pretrained knowledge. *arXiv preprint arXiv:2505.21906*, 2025. [2](#)
- [53] Xiang Zhu, Yichen Liu, Hezhong Li, and Jianyu Chen. Learning generalizable robot policy with human demonstration video as a prompt. *arXiv preprint arXiv:2505.20795*, 2025. [2](#)
- [54] Yichen Zhu and Feifei Feng. Let me show you: Learning by retrieving from egocentric video for robotic manipulation. *arXiv preprint arXiv:2511.05199*, 2025. [2](#)
- [55] Brianna Zitkovich, Tianhe Yu, Sichun Xu, Peng Xu, Ted Xiao, Fei Xia, Jialin Wu, Paul Wohlhart, Stefan Welker, Ayzaan Wahid, et al. Rt-2: Vision-language-action models transfer web knowledge to robotic control. In *Conference on Robot Learning*, pages 2165–2183. PMLR, 2023. [2](#)

A. World in Your Hand (WiYH) Dataset

A.1. Detailed Task-Skill Counting Statistics

- We further supplement the visualization of the number of skills corresponding to each task. Due to space limitations, we report statistics based on only 25% of the dataset, as shown in Figure 16. The full visualization analysis will be updated subsequently on the dataset website.

A.2. Additional annotation examples visualizations

- We provide additional annotation visualizations for the remaining 6 scenes, as shown in Figure 15.

A.2.1. Data Annotation Details.

Raw videos are structured into a three-tier hierarchy: Scene - Task - Subtask by Annotators. Each subtask corresponds to the minimal object-centered action unit or a temporally cohesive action sequence. **(1) Subtask Annotation:**

- **Actions:** Drawn from predefined operation sets (e.g., PICK, PLACE_INTO, SEARCH).
- **Target Object:** Semantic structure describing action objects and positional relationships (e.g., [object, container]).
- **Temporal Bounds:** Precise start/end timestamps delimiting the execution segment in the video.
- **Status:** Labeled as success, failure, irrelevant to denote execution outcome.

(2) Subtask Prediction chain-of-thought (CoT): With the subtask annotation, we select tasks of moderate length (containing 4-10 subtasks). We annotate them with Chain-of-Thought data, providing reasoning that decomposes the task into several logically connected subtasks. The annotation pipeline for CoT is illustrated in Figure 10. Initially, we provide the model (Qwen2.5-VL) with both the current subtask information (video and text) and the ground-truth text of the next subtask. The model is then prompted to perform posterior attribution, explaining why the specified next subtask logically follows. Subsequently, the attribution is appended to the input and presented again to Qwen2.5-VL, which synthesizes it into a structured causal reasoning process. Finally, the CoT segment is extracted and used to prompt Qwen-3, which is instructed to predict an answer. This predicted answer is matched against the ground-truth answer to validate the completeness and soundness of the CoT labeling.

B. Benchmark Details

B.1. Human-centric Vision-Language

B.1.1. Benchmark Task Descriptions.

The Human-centric Vision-Language Benchmark in Section 3.1 is constructed by sampling raw data from WiYH,

followed by manual annotation, including Spatial Referring, Subtask Prediction, and Completion Verification, with distributions illustrated in Figure 9. (1) The Spatial Referring is designed as a spatial region grounding form: given relevant image frames, annotators delineate ROI areas using polygons according to the given questions. It evaluates spatial understanding by prompting the model to output a set of points representing the spatial region referenced in the question. The primary metric is the proportion of these points that fall within the ground-truth polygon. (2) The Subtask Prediction adopts a multiple-choice question format. Using Qwen2.5-VL-72B, we first generate 9 negative candidate options based on video segments and ground truth, spanning action, object, and orientation dimensions. Annotators then manually select the top three hard negative samples, which, together with the correct answer, form the final candidate set. (3) The Completion Verification is designed as binary questions: given a video segment randomly truncated from the end, annotators determine whether the subtask has been completed. And this evaluation metric is the selection accuracy rate.

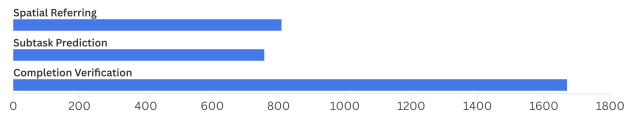


Figure 9. Amount of three task annotations in the Human-centric Vision-Language Benchmark.

B.1.2. Benchmark Tasks Visualization.

Examples of the three tasks are shown in Figure 11.

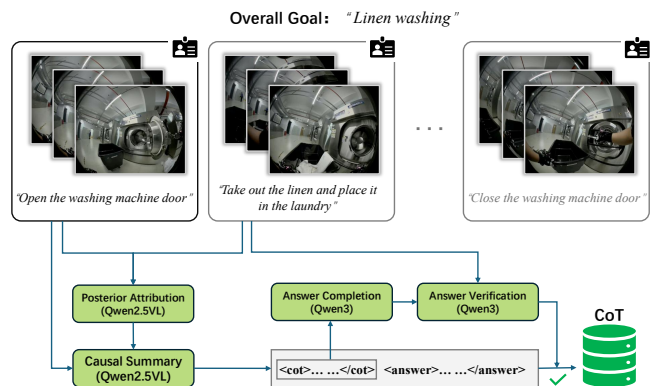


Figure 10. The annotation pipeline for subtask prediction chain-of-thought (CoT).

B.2. Human-centric World Model

B.2.1. Language-conditioned Video Generation

Baseline. We validate the effectiveness of our WiYH dataset using video generation baselines with different architectures, including transformer (CogVideo [18]) and U-Net (DynamiCrafter [48]).

Evaluation Metrics. Following VBench [21], the evaluation metrics are as follows:

- **Consistency.** To evaluate the temporal consistency of the target manipulation subjects, we calculate the DINO [10] feature similarity across frames. For assessing the temporal consistency of the background scenes, we compute the CLIP [36] feature similarity across frames. The overall consistency score is defined as the arithmetic mean of the subject consistency and the background consistency.
- **Smoothness.** To assess the temporal continuity of the generated videos, we employ a motion-consistency metric based on the AMT [31] video frame interpolation model. Given a generated video with frames $\{f_0, f_1, \dots, f_{2n-1}, f_{2n}\}$, we first remove all odd-indexed frames to obtain $\{f_0, f_2, \dots, f_{2n}\}$. The AMT model is then used to interpolate the missing frames, producing $\{\hat{f}_1, \hat{f}_3, \dots, \hat{f}_{2n-1}\}$. Finally, we compute the mean absolute error between the interpolated and original frames, where a larger value indicates smoother and more temporally coherent motion.
- **Dynamic.** To prevent the model from producing static videos in pursuit of higher temporal consistency scores, we employ RAFT [38] to estimate optical flow strengths between consecutive frames of each generated video. The average of the largest 5% optical flows is used to determine whether the video is static. The final dynamic score is calculated by measuring the proportion of non-static videos generated by the model.
- **Quality.** To assess the visual quality of generated video frames, we employ the MUSIQ [24] image quality predictor trained on the SPAQ [14] dataset. This metric quantifies common distortions such as overexposure, noise, and blur, with a higher score indicating fewer artifacts.

Implementation Details. During fine-tuning, all input videos are resized to 480p resolution. For CogVideo, we use the pre-trained image-to-video version with a temporal length of 49, a learning rate of $2e-5$, and a batch size of 16. For Dynamicrafter, we leverage the model pre-trained at 512 resolution, setting the temporal length to 48, the learning rate to $1e-5$, and the batch size to 16.

B.2.2. Gaussian Splatting 4D Reconstruction

Evaluation Metrics. In terms of metrics of 4D reconstruction, we evaluate the RGB rendering quality using PSNR, SSIM, and LPIPS. For PSNR and SSIM, higher is better, while for LPIPS, lower is better. For geometry accuracy from rendered depth maps, we use A.R. (lower is better)

and δ_1 (higher is better).

- PSNR (Peak Signal-to-Noise Ratio),

$$\text{PSNR} = 10 \cdot \log_{10} \left(\frac{\text{MAX}_I^2}{\text{MSE}} \right)$$

$$\text{MSE} = \frac{1}{MN} \sum_{i=1}^M \sum_{j=1}^N (I(i, j) - K(i, j))^2,$$

where I is the reference image, K is the rendered image, and MAX_I is the maximum possible pixel value. A higher PSNR indicates that the rendered image is closer to the ground truth.

- SSIM (Structural Similarity Index Measure).

$$\text{SSIM}(x, y) = \frac{(2\mu_x\mu_y + c_1)(2\sigma_{xy} + c_2)}{(\mu_x^2 + \mu_y^2 + c_1)(\sigma_x^2 + \sigma_y^2 + c_2)},$$

where μ , σ , and σ_{xy} denote the mean, variance, and covariance of image patches x and y , respectively. SSIM evaluates perceptual similarity in terms of luminance, contrast, and structure; values closer to 1 indicate better similarity.

- LPIPS (Learned Perceptual Image Patch Similarity). This metric computes the perceptual distance between rendered and ground-truth images by extracting deep features from a pretrained CNN and measuring the distance in that feature space. Lower LPIPS values indicate that two images are more perceptually similar.
- AbsRel (Absolute Relative Error).

$$\text{AbsRel} = \frac{1}{N} \sum_{i=1}^N \frac{|d_i - d_i^*|}{d_i^*},$$

where d_i is the predicted depth at the pixel i and d_i^* is the corresponding ground-truth depth. A lower value denotes a more accurate geometry.

- δ_1 (Threshold Accuracy / Delta1).

$$\delta_1 = \frac{1}{N} \sum_{i=1}^N \mathbf{1} \left(\max \left(\frac{d_i}{d_i^*}, \frac{d_i^*}{d_i} \right) < 1.25 \right),$$

which measures the percentage of predicted depth values that are within a factor of 1.25 of the ground-truth depth. A higher value δ_1 indicates better accuracy.

Implementation Details. During optimization, all input videos are processed at a resolution of 960×720 . We represent each scene with 40k dynamic Gaussians and 100k static Gaussians and use $B = 10$ shared SE(3) motion bases for all points. We optimize the model with Adam, running 1k iterations for the initialization stage and 500 training epochs, with learning rates of 1.6×10^{-4} for Gaussian means and SE(3) bases, 5×10^{-3} for scales, 1×10^{-3} for rotations, and 1×10^{-2} for colors, opacities, and motion coefficients. Training on a 300-frame sequence takes about 2 hours on a single A100 GPU and supports real-time rendering at around 140 FPS.

B.3. Details of Cross-Embodiment Analysis.

In this section, we present the details of our cross-embodiment experiments in Section 4, Cross-Embodiment Analysis, of the main text. As shown in Figure 14, we demonstrate 11 task variants under two scenarios: Single-Object Scene and Multi-Object Cluttered Scene. Figures 12 and 13 illustrate the success rates and failure causes for each task in these two scenarios, respectively.

As shown in Figures 12 and 13, on most tasks, the incorporation of human data leads to a general increase in success rate. In the Single-Object Scene, the diverse action distribution of human data enhanced the policy’s generalization capability to unseen initial states, enabling successful grasping at different positions or over long distances. In the Multi-Object Cluttered Scene, policies trained solely on UMI data demonstrated almost no generalization ability in complex scenarios. When factors such as object height or layout changed, policies trained only on UMI data failed, whereas the inclusion of human data gradually enabled success by effectively introducing both the action and observation domains of human data into the robot dataset.

Furthermore, the consistently low success rates across all methods in certain tasks highlight important directions for future research: how to further improve the collection precision of human data and how to design efficient algorithms that can better transfer knowledge from human data to dexterous manipulation tasks.

C. Ethics and Privacy Statement

Our work involves large-scale data collection of real-world human manipulation activities. We took a number of measures to ensure responsible data handling, privacy protection, and ethical compliance.

Data Collection and Consent. All human subjects participating in data collection were recruited voluntarily and provided informed consent in accordance with institutional guidelines. Participants were briefed on the purpose of the study, the modalities collected (RGB video, depth, motion capture, tactile sensing), the intended research use, and their right to withdraw at any time.

Privacy Protection. Although the dataset contains real-world human activities and may capture visible human faces or identifiable biometric patterns, several privacy-preserving strategies were implemented:

- **Controlled subjects only:** No bystanders or non-consenting individuals appear in the dataset; all scenes were recorded in controlled environments with only consenting operators present.
- **No identity labels:** We do not include personal information, demographic information, or identity annotations.
- **Face and identity protection:** When faces are visible in RGB streams, we apply optional face blurring in the pub-

lic release version.

- **No audio recordings:** We do not collect speech or audio signals to avoid unintended disclosure of personal information.

Sensitive Content and Safety. The dataset does not include minors, hazardous behaviors, or sensitive activities. All recordings were conducted in standard workplace or daily-life environments using safety protocols.

Data Usage and Licensing. The released dataset is intended exclusively for research on embodied AI, manipulation, perception, and VLA learning. Redistribution or commercial use is restricted according to the license accompanying the dataset. Users are required to comply with ethical research practices and avoid any attempts at identity recognition or misuse of human-related data.

Potential Risks and Mitigations. As with any dataset containing human recordings, there is a theoretical risk of model misuse, such as identity extraction or surveillance applications. To mitigate these risks, we provide: (1) no textual identity metadata, (2) optional visual anonymization tools, and (3) a license that explicitly forbids re-identification, face recognition, or surveillance-related uses.

Institutional Review. All data collection procedures were reviewed and approved by an internal ethics committee to ensure compliance with privacy protection and responsible AI principles.

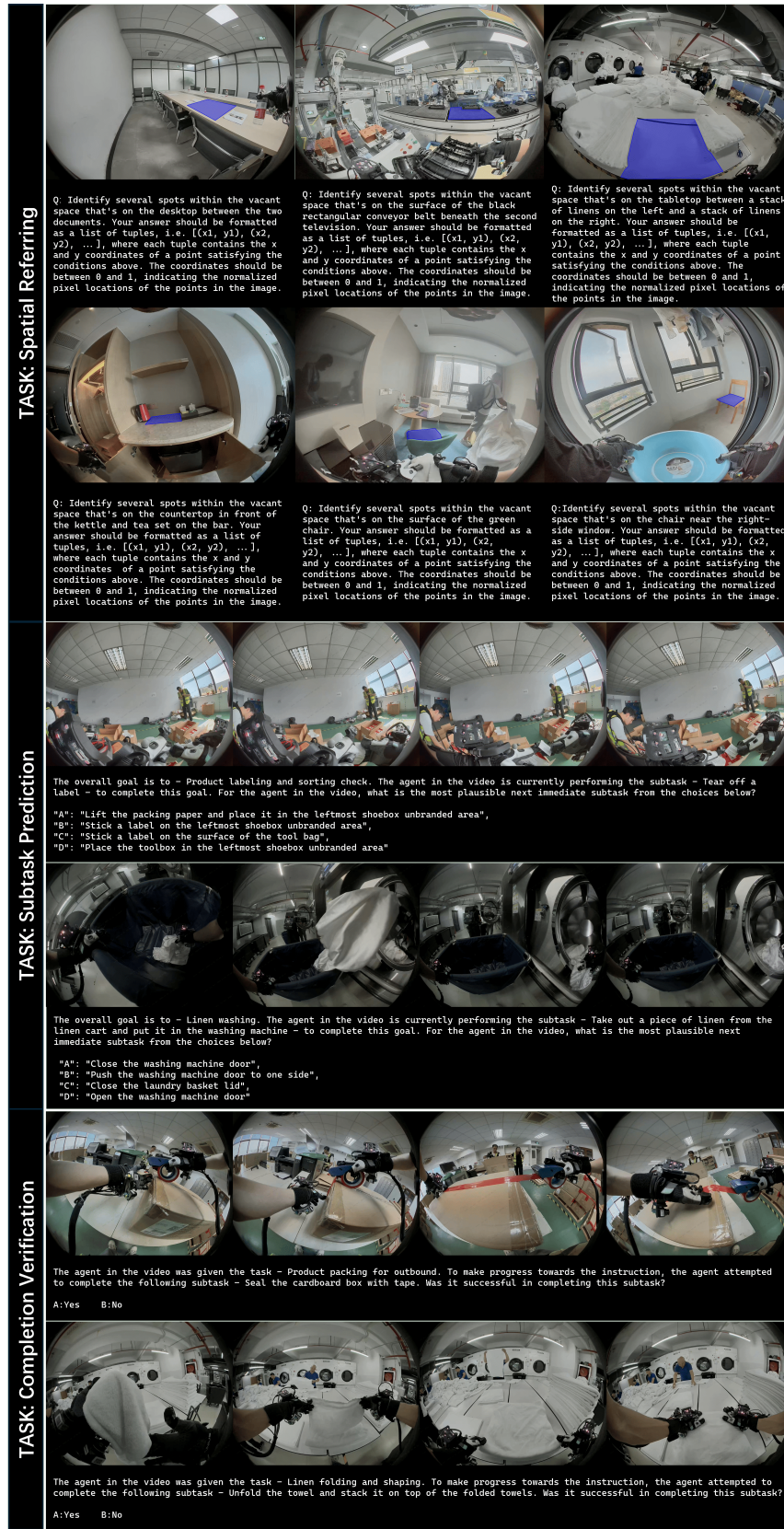


Figure 11. Examples of three task annotations in the Human-centric Vision-Language Benchmark.

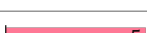
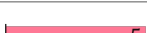
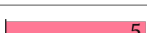
Task Variation	Training Recipe	Failure Analysis	Success vs. Failure
(1) Grasping from HOME_POINT with the target in front of hand.	UMI#200	Failed to reach a reasonable position, early grasping	
	UMI#500	Grasped air	
	UMI#200+WiYH#800	Failed to reach a reasonable position, early grasping	
	UMI#500+WiYH#800	-	
(2) Grasping from HOME_POINT with the target in right, front of hand.	UMI#200	Far distance, can not grasping	
	UMI#500	Failed to reach a reasonable position, early grasping	
	UMI#200+WiYH#800	Failed to reach a reasonable position, early grasping	
	UMI#500+WiYH#800	Failed to reach a reasonable position, early grasping	
(3) Grasping from HOME_POINT with the target in right, front of hand, away from hand.	UMI#200	Large positional deviation	
	UMI#500	Significant deviation from the target	
	UMI#200+WiYH#800	Failed to reach a reasonable position, collided with target	
	UMI#500+WiYH#800	Reached the position, unreasonable grasp timing	
(4) Grasping from HOME_POINT with the target in middle of platform, parallel to the hand.	UMI#200	Unable to reach the grasping position	
	UMI#500	Unable to reach the grasping position	
	UMI#200+WiYH#800	Collided with the target	
	UMI#500+WiYH#800	Failed to reach a reasonable position, early grasping, collided	
(5) Grasping from HOME_POINT with the target in left of hand, close to the hand.	UMI#200	Collided with the target	
	UMI#500	Severe finger compression	
	UMI#200+WiYH#800	Collided with the target	
	UMI#500+WiYH#800	Failed to reach a reasonable position, early grasping, collided	
(6) Hand facing to the target directly.	UMI#200	Joint and motion anomalies	
	UMI#500	Failed to reach a reasonable position, early grasping, collided	
	UMI#200+WiYH#800	Collided with the target	
	UMI#500+WiYH#800	Collided with the target	

Figure 12. Cross-embodiment Manipulation Details - 1.

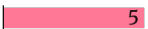
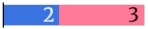
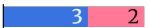
Task Variation	Training Recipe	Failure Analysis	Success vs. Failure
(7) Crowded objects around the target.	UMI#200	Abnormal grasping behavior	 5
	UMI#500	Failed to reach a reasonable position, early grasping, collided	 2 3
	UMI#200+WiYH#800	Failed to reach a reasonable position, early grasping, collided	 3 2
	UMI#500+WiYH#800	Failed to reach a reasonable position, early grasping, collided	 4 1
(8) Obstacle in front of the target.	UMI#200	Abnormal grasping behavior	 5
	UMI#500	Unable to reach the target position	 5
	UMI#200+WiYH#800	Grasping position too low, collided with other assets	 2 3
	UMI#500+WiYH#800	Severe finger compression	 3 2
(9) Elevated the target.	UMI#200	Abnormal grasping behavior	 5
	UMI#500	Unable to reach the grasping position	 5
	UMI#200+WiYH#800	Reached the grasping position, grasping failed	 3 2
	UMI#500+WiYH#800	Severe finger compression	 5
(10) Elevated the target, hand facing to the target directly.	UMI#200	Unable to reach the grasping position	 5
	UMI#500	Unable to reach the grasping position	 5
	UMI#200+WiYH#800	Failed to reach a reasonable position, early grasping	 5
	UMI#500+WiYH#800	-	 5
(11) leaned target.	UMI#200	Unable to reach the grasping position	 5
	UMI#500	Incorrect grasping location	 5
	UMI#200+WiYH#800	Incorrect grasping location	 5
	UMI#500+WiYH#800	Incorrect grasping location	 3 2

Figure 13. Cross-embodiment Manipulation Details - 2.



Figure 14. Task variant visualization in the cross-embodiment Manipulation.

